Chemical Physics Letters 831 (2023) 140857

Contents lists available at ScienceDirect

Chemical Physics Letters

journal homepage: www.elsevier.com/locate/cplett

# Theoretical re-investigation on the N–N bond breaking of $N_2O^+$ cations in the $A^2\Sigma^+$ and $B^2\Pi$ states at the CASPT2 level

Yan Chen [a,1], Xiangkun Wu [b,1], Tongpo Yu [a], Xiaoguo Zhou [a,*], Bing Yan [c,*], Shilin Liu [a]

[a] Department of Chemical Physics, University of Science and Technology of China, Hefei 230026, China
[b] Paul Scherrer Institute, 5232 Villigen, Switzerland
[c] Institute of Atomic and Molecular Physics, Jilin University, Changchun 130012, China

ARTICLE INFO

*Keywords:*
Potential energy surfaces
Decomposition
Avoided crossing
Spin-orbit coupling
Ro-vibrational distributions

ABSTRACT

Two-dimensional multistate potential energy surfaces along N–NO bond length and N–N–O bond angle of $N_2O^+$ in the $A^2\Sigma^+$ and $B^2\Pi$ states were calculated at the CASPT2/cc-pVQZ level. In comparison to the known decomposition mechanisms in linear structure, a new N–NO bond fission pathway was proposed in bent geometry for the $A^2A'(A^2\Sigma^+)$ state with a lower barrier, leading to rotationally excited $NO^+(X^1\Sigma^+)$ and $N(^2D)$ fragments. Likewise, the respective contributions of the A' and A'' components split from the $B^2\Pi$ state were clarified. Considering avoided crossing and the coupling of spin states, ro-vibrational distributions of the $NO^+$ fragment ion observed in experiments are elucidated.

## 1. Introduction

Nitrous oxide ($N_2O$), an asymmetric linear triatomic molecule, plays a significant role on combustion chemistry [1], atmospheric chemistry [2] and medicine [3]. The corresponding cation, $N_2O^+$, was observed as an intermediate of widely concerned ion-molecular reactions in the ionospheres of Earth, Mars, and Venus [4]. Herein, the geometries and dynamics of $N_2O$ and its cation have received wide attentions.

The electronic configurations and vibrational structures of $N_2O^+$ in lowest-lying valence states like $X^2\Pi$, $A^2\Sigma^+$, $B^2\Pi$, $C^2\Sigma^+$ and $D^2\Pi$, were extensively studied with many experimental approaches, such as photoelectron spectroscopy (PES) [5–10], threshold photoelectron spectroscopy (TPES) [11–15], pulsed filed ionization-photoelectron spectroscopy (PFI-PES) [16–18] and photofragment excitation (PHOFEX) spectroscopy [19]. Moreover, dissociation dynamics of $N_2O^+$ in low-lying electronic states were experimentally investigated using electron ionization mass spectrometry [20–22], photoionization mass spectrometry [23–26], velocity map imaging of photofragments [27], fast-ion-beam laser spectroscopy [28,29], photoelectron-photoion coincidence (PEPICO) [30–32], threshold photoelectron-photoion coincidence (TPEPICO) [11–14,33], and photoelectron-photoion vector correction [34,35]. From these experiments, a consistent conclusion is drawn that the ground state, $X^2\Pi$, is typically bound along the N–O or N–N coordinates, while the excited states including $A^2\Sigma^+$, $B^2\Pi$, $C^2\Sigma^+$ and $D^2\Pi$ are all predissociative, except for a few lowest vibrational levels of $A^2\Sigma^+$ [12,15,27,33,36,37]. For $N_2O^+$ ions in the $A^2\Sigma^+$ state, bimodal rotationally distributed $NO^+$ fragments were distinctly observed along the $NO^+(X^1\Sigma^+) + N(^2D)$ decomposition pathway, besides the lowest $NO^+(X^1\Sigma^+) + N(^4S)$ one [27]. Likewise, the decomposition of $N_2O^+$ in the $B^2\Pi$ state mainly leaded to $N(^2D)$ and $NO^+(X^1\Sigma^+)$ fragments, and significant bending took place prior to the dissociation of parent ions [34,37].

In contrast to the above experiments, theoretical computations on molecular structures, vibrational frequencies and dissociation mechanisms of $N_2O^+$ ion in low-lying electronic states are relatively limited. In 2000, Chambaud et al. [38] performed *ab initio* calculations on the decomposition mechanism of $N_2O^+(A^2\Sigma^+)$ ions using complete active space self-consistent field (CASSCF) and multi-reference configuration interaction (MRCI) methods. Predissociation of $A^2\Sigma^+$ was suggested to occur in bent geometry through spin–orbit coupling (SOC) with $1^4\Pi(^4A'')$ state, which the lowest dissociation channel of $NO^+(X^1\Sigma^+) + N(^4S)$ was adiabatically correlated to. Moreover, there was a crossing on potential energy surfaces between the $A^2\Sigma^+$ and $B^2\Pi$ states in linear geometry, and both of them could vibronically coupled according to the bending mode [38]. Using multi-reference second-order perturbation theory (CASPT2), Huang and his co-workers [39] calculated the one-dimensional cuts of potential energy surfaces for the $X^2\Pi$, $1^4\Sigma^-$, and

* Corresponding authors.
*E-mail addresses:* xzhou@ustc.edu.cn (X. Zhou), yanbing@jlu.edu.cn (B. Yan).
[1] These authors contributed equally to this work

https://doi.org/10.1016/j.cplett.2023.140857
Received 31 May 2023; Received in revised form 26 September 2023; Accepted 27 September 2023
Available online 3 October 2023

$1^4A''$ states of $N_2O^+$ along $N_2$-O and N–NO coordinates, respectively. They proposed the adiabatic and non-adiabatic dissociation mechanisms to produce $NO^+(X^1\Sigma^+)$ and $N(^4S)$, and $N_2(X^1\Sigma^+)$ and $O^+(^4S)$ fragments. Soon afterwards, they revised two predissociation mechanisms of the N-loss process from $N_2O^+(A^2\Sigma^+)$ [40]. In $C_s$ symmetry (bent geometry), $A^2\Sigma^+(2^2A')$ linked with the $NO^+(X^1\Sigma^+)$ + $N(^4S)$ channel through SOC with $1^4A''$, while it could also dissociate to $NO^+(X^1\Sigma^+)$ and $N(^2D)$ fragments via two SOCs of $2^2A'/1^4A''$ and $1^4A''/X^2\Pi(1^2A'')$ [40]. No theoretical studies on the higher electronic states have been reported to date.

Notably, for triatomic ion-molecular intermediates, the bending sometimes shows a decisive influence in dissociation pathways [41–43]. According to the experimental conclusions of the $B^2\Pi$ and $D^2\Pi$ decomposition [15,34,37], the linear-to-bent geometrical change might occur prior to the N–NO bond fission. Therefore, more details of potential energy surfaces of $N_2O^+$ in bent excited states are necessary to verify these inferences. Our attention in this work is focused on the N–NO bond breaking mechanism of $N_2O^+$ cation without linear geometry constraint. Based on the calculated geometries and energies using the CASPT2 approaches, we plot two-dimensional (2D) multistate potential energy surfaces of these electronic states, along the N–N bond length and bond angle coordinates. Considering SOC effects, we propose plausible mechanisms of N–NO bond breaking for $N_2O^+$ in the $A^2\Sigma^+$ and $B^2\Pi$ states.

## 2. Theoretical methods

All quantum chemical calculations were performed using MOLPRO version 2021.3 program [44]. Electronic configurations and transition characteristics of the low-lying electronic states of $N_2O^+$ cation were analyzed, based on the CASSCF wavefunctions. As the molecular electronic configuration of the neutral $N_2O$ ground state is $(1\sigma)^2(2\sigma)^2(3\sigma)^2(4\sigma)^2(5\sigma)^2(6\sigma)^2(1\pi)^4(7\sigma)^2(2\pi)^4(3\pi)^0(8\sigma)^0(9\sigma)^0$, the full valence active space including the 4σ-9σ and 1π-3π orbitals was chosen, and 16 electrons for neutral and 15 electrons for cations were active, i.e. CASSCF(15,12) for $N_2O^+$. To investigate the dissociation mechanism of the $A^2\Sigma^+$and $B^2\Pi$ states, the lowest eight A' and four A'' states in $C_S$ symmetry (bent geometry) were chosen to calculate at the multi-state multi-reference (MS-MR) CASPT2 level [45]. All calculations, including geometric optimization and single point energy calculation, were performed at the CASPT2 level with the cc-pVQZ basis set [46].

Considering that the bending mode might have significant influence on the related decomposition dynamics, 2D potential energy surfaces along the N–NO bond length and the N–N–O angle with the intervals of 0.05 Å and 5° were calculated at the MS-MR CASPT2 level to clarify dissociation mechanisms. Moreover, the potential energy surfaces were not fitted, resulting in a slight lack of smoothness. According to the fact that only a minor variation occurs for the N–O bond length in photoionization and dissociative photoionization of $N_2O$ (Table 2), it is reasonable to maintain this distance at 1.189 Å as its value in neutral molecule for economy when scanning the N–NO bond length and the N–N–O angle. In addition, only potential energy surfaces in Franck-Condon (FC) region are concerned in current multi-reference calculations, since the couplings with higher excited states usually occur far from the FC region and however the high rates of motion for fragments naturally undermine their effects on the real dissociation dynamics. Specifically, the FC region was approximated to be taken as the N–N bond length of 1.06–1.21 Å and the N–N–O bond angle of 159-180°, according to the zero-point energy on the potential energy surface of the neutral $N_2O$ along the N–N bond length and the N–N–O bond angle.

## 3. Results and discussion

### 3.1. Electronic states properties of $N_2O^+$ in low-lying states

By removing an electron from the outer orbitals of neutral molecule, $N_2O^+$ in the $X^2\Pi$, $A^2\Sigma^+$, $B^2\Pi$, and $C^2\Sigma^+$ states can be produced. Table 1 summarizes the major electronic configurations (with coefficients of larger than 0.30) of each low-lying state, based on CASSCF wavefunction analyses. Apparently, the $X^2\Pi$ state is classified into a primary ionization state (PIS) by simply removing a 2π electron, while the $A^2\Sigma^+$, $B^2\Pi$, and $C^2\Sigma^+$ states all have the multi-configuration (TMC) features. Notably, the previous *ab initio* Tamm-Dancoff calculations demonstrated that strong vibronic coupling through totally symmetric vibrational modes could be induced by the electron correlation between the $(1\pi_x)^{-1}$ and $(2\pi_x)^{-2}(3\pi_x)^{+1}$ components for the $B^2\Pi$ state [47], where minus sign means to remove electrons while positive one indicates that the orbital is filled with an electron. In addition, electrons correlation inevitably occurs between the $A^2\Sigma^+$ and $C^2\Sigma^+$ states due to their similar electronic configurations, suggesting that we need to pay attention to their coupling in the dissociation process.

### 3.2. Optimized geometries of $N_2O^+$ in the $A^2\Sigma^+$ and $B^2\Pi$ states

Table 2 lists the CASPT2 optimized geometries and excitation energies of $N_2O^+$ in the $X^2\Pi$, $A^2\Sigma^+$ and $B^2\Pi$ states, as well as the previously reported data. At the same level of theory, we also calculated the optimized geometry of neutral $N_2O$ molecule in ground state, in which the R (N–N) and R(N–O) bond lengths were 1.133 and 1.189 Å, respectively, and the θ(N–N–O) was 180.0°. Apparently, the N–O bond length remains almost unchanged in photoionization to the lower ionic states such as the $X^2\Pi$, $A^2\Sigma^+$ and $B^2\Pi$, which is also close to its value (1.067 Å) in $NO^+(X^1\Sigma^+)$ fragment. Besides, as a linear $^2\Pi$ state will split into two sub-states of A' and A'' symmetry in bent geometry, the $X^2\Pi$ and $B^2\Pi$ states each correlate with two sub-states in $C_S$ symmetry, e.g. $B^2A'$ and $B^2A''$. It is worth noting that the major aim of the current calculations is to unravel 2D potential energy surfaces of the $A^2\Sigma^+$ and $B^2\Pi$ states, rather than to obtain high precision excitation energies. Therefore, a systematic error of ~ 0.20 eV for excitation energies in Table 2 is acceptable in comparison to experimental data.

As shown in Table 2, the $X^2\Pi$ and $A^2\Sigma^+$ states have linear geometries, and the present geometrical parameters are also close to previous results [40]. Two sub-state components of $X^2\Pi$ remain degenerate in the FC region. Moreover, the two bond lengths of $N_2O^+$ in the $X^2\Pi$ and $A^2\Sigma^+$ states are both close to those of the neutral molecule, which agrees with the experimental phenomenon that the strongest peak of both photoelectron spectral bands is located at the vibrational ground level ($v^+$=0) [11,18,50]. The vertical (VIE) and adiabatic (AIE) ionization energies of $N_2O$ molecule are calculated to be 12.76 and 12.62 eV, respectively, which generally agrees with the experimental (12.89 eV [49]) and theoretical (12.80 eV [34]) data of VIE. The adiabatic excitation energy ($T_0$) of $A^2\Sigma^+$ is calculated to be 3.34 eV, which is also consistent with the previously calculated (3.29 eV [40]) and experimental values (3.50 eV [48]).

The degeneracy of the $B^2\Pi$ is broken in bent geometry, and two sub-states exhibit obvious difference in optimized geometries and excitation energies. The $B^2A'$ remains linear, and the N–N and N–O bond lengths are calculated to be 1.248 and 1.278 Å, respectively. In contrast, the $B^2A''$ sub-state is bent with θ(N–N–O) = 121.4°, R(N–N) = 1.315 Å and R (N–O) = 1.197 Å. To our surprise, in addition to the same VIEs for the

**Table 1**
CASSCF wavefunction of $N_2O^+$ in low-lying electronic states, at the optimized geometry of neutral molecule in the ground state.

| State Linear | **Bent** | electronic configuration | coefficient | characteristics |
|---|---|---|---|---|
| $X^2\Pi$ | $1^2A', 1^2A''$ | $(2\pi_x)^{-1}$ | 0.917 | PIS |
| $A^2\Sigma^+$ | $2^2A'$ | $(7\sigma)^{-1}$ | 0.739 | TMC |
| | | $(6\sigma)^{-1}$ | 0.445 | |
| $B^2\Pi$ | $3^2A', 2^2A''$ | $(1\pi_x)^{-1}$ | 0.774 | TMC |
| | | $(2\pi_x)^{-2}(3\pi_x)^{+1}$ | 0.391 | |
| $C^2\Sigma^+$ | $4^2A'$ | $(7\sigma)^{-1}$ | 0.513 | TMC |
| | | $(6\sigma)^{-1}$ | 0.731 | |

**Table 2**
Optimized geometries, ionization energies and adiabatic excitation energies of $N_2O^+$ in low-lying electronic states.

| state | N–N /Å | N–O /Å | θ(N–N–O) /° | IE /eV VIE | AIE | $T_0$ /eV calc.[a] | exp. |
|---|---|---|---|---|---|---|---|
| $X^2\Pi$ | 1.148 | 1.194 | 180.0 | 12.76 | 12.62 | 0.00 | 0.00 |
| | 1.154[b] | 1.185[b] | | | 12.89[c] | | |
| $A^2\Sigma^+$ | 1.134 | 1.152 | 180.0 | 16.13 | 15.97 | 3.34, 3.29[f] | 3.50 [g] |
| | 1.140[b] | 1.141[b] | | | 16.39[d,e] | | |
| $B^2A''(B^2\Pi)$ | 1.315 | 1.197 | 121.4 | 17.91 | 16.16 | 3.48 | |
| $B^2A'(B^2\Pi)$ | 1.248 | 1.278 | 180.0 | 17.91 | 17.15 | 4.46 | 4.7 [g] |

a. with zero-point-energy corrections using the vibrational frequencies at the CASSCF level; b. calculated by the moments of inertia in Ref. [48]; c. in He-I photoelectron spectroscopy of Ref. [49]; d. in TPES of Ref. [11]; e. in PFI-ZEKE-PES of Ref. [50]; f. calculated at CASPT2 level in Ref. [40]; g. in photoelectron spectroscopy of Ref. [51].

$B^2A''$ and $B^2A'$ sub-states, there is a big gap between their AIE values, since the $T_0$ values of $B^2A''$ and $B^2A'$ are calculated to be 3.48 and 4.46 eV, respectively. Notably, a series of vibrational peaks were observed in the $B^2\Pi$ energy range of photoelectron spectra [9], which were attributed to the dominant excitation of symmetric stretching mode ($\nu_1^+$). Moreover, the experimental origin of the $B^2\Pi$ band was close to the calculated AIE of $B^2A'$ [9]. These results strongly indicate that the experimental $B^2\Pi$ band is predominantly contributed by the ionization transition to the $B^2A'$ sub-state. Therefore, the decomposition of $N_2O^+(B^2\Pi)$ will principally occur along the potential energy surface of $B^2A'$ sub-state, while the contribution of $B^2A''$ component is minor.

### 3.3. Potential energy surface of the $A^2\Sigma^+(2^2A')$ state

We initially calculated the 2D multistate potential energy surfaces in the FC region of low-lying doublet states involving the lowest eight A' and four A'' states, using the MS-MR CASPT2 method. Fig. S1 plots the cut-off potential energy curves of these low-lying excited states in quasi-linear geometry with the fixed θ(N–N–O) of 179.9°, where several N–NO dissociation limits are noted. Because the potential energy surface of the linear $X^2\Pi$ ionic state is well known, only the electronically excited states are discussed here.

The linear $A^2\Sigma^+(2^2A')$ state was assigned to adiabatically correlate with the third dissociation limit of $NO^+(X^1\Sigma^+) + N(^2P)$ in the previous calculation [40], with a very high barrier (3.31 eV). When the linear configuration of $N_2O^+$ is broken, complicated couplings between electronic states with same symmetry, e.g. $A^2\Sigma^+(2^2A')$ and $B^2A'$, are involved in CASPT2 calculations, leading to new adiabatic dissociation pathways. As shown in the 2D multistate potential energy surfaces of $^2A'$ symmetry of Fig. 1a, there are two strong coupling regions on the quasi-linear $A^2\Sigma^+(2^2A')$ potential energy surface: one is located near the bottom of $B^2A'$ state between $A^2\Sigma^+(2^2A')$ and $B^2A'$ (noted with yellow sand clock), and the other is at R(N–N) = 1.80 Å between $A^2\Sigma^+(2^2A')$ and an upper A' state. Notably, the former can lead to the avoided crossing between $B^2A'$ and $A^2A'$ states, in line with Chambaud et al.'s calculations [38]. Actually, this coupling provides a non-adiabatic decomposition pathway for $N_2O^+(B^2A')$ via the $A^2\Sigma^+(2^2A')$ state. Moreover, these couplings make the dominant electronic configuration of $A^2\Sigma^+(2^2A')$ exchanged along the N–NO bond rupture. As a result, the linear $A^2\Sigma^+(2^2A')$ adiabatically links with the lower dissociation limit of $NO^+(X^1\Sigma^+) + N(^2D)$, which is different from the previous conclusion [40]. The forming barrier height is calculated to be 2.2 eV. Although this barrier is much lower than that in linear geometry, it is still too high to allow the linear decomposition of $A^2\Sigma^+(2^2A')$.

An important finding is the first-ever discovery of a local minimum (named as LM-$2^2A'$ in Fig. 2) on the $A^2\Sigma^+(2^2A')$ potential energy surface, which is far away from the FC region. We liberalize the restriction on the N–O bond length, and the optimized geometry of LM-$2^2A'$ has the N–N bond length of 1.312 Å, the N–O bond length of 1.195 Å and the bond angle of 115.0°, as shown in Fig. 3. The $T_0$ value of LM-$2^2A'$ is 3.36 eV and slightly higher than the global minimum. The electronic configuration property of LM-$2^2A'$ changes from TMC in the linear geometry to PIS with the dominant configuration of $(2\pi)^{-2}(3\pi)^{+1}$ with the coefficient of 0.879. There is a transition state (TS-$2^2A'$) between the local and global minima, whose optimized geometry is also exhibited in Fig. 3. Notably, this isomerization barrier is only 0.62 eV and much lower than the linear barrier height. Therefore, the existence of the local minimum and the lower barrier strongly imply a novel adiabatic pathway for the $N_2O^+(A^2\Sigma^+)$ decomposition, as marked with red arrow in Fig. 2. Along

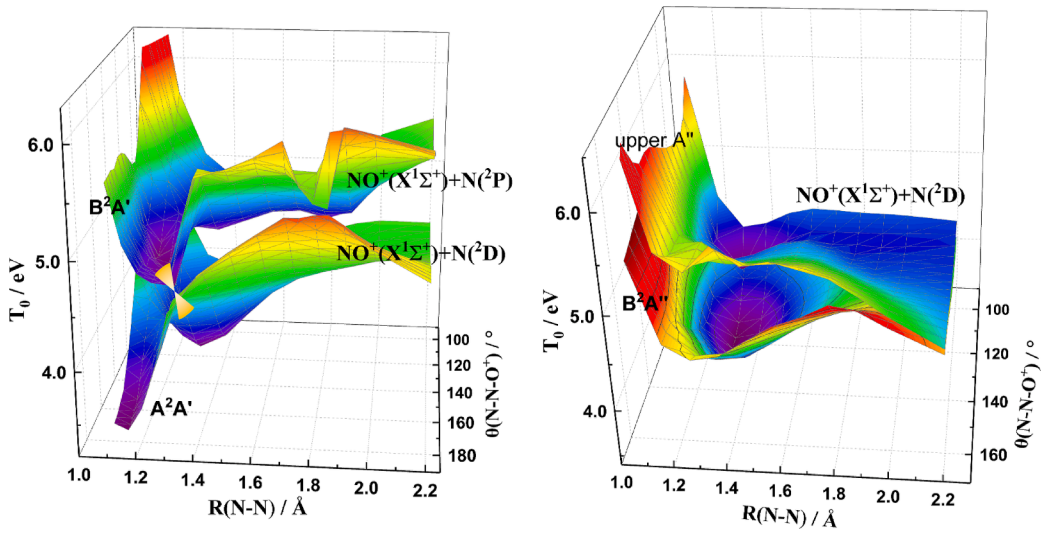


**Fig. 1.** 2D multistate CASPT2 potential energy surfaces of the low-lying A' (a) and A'' (b) sub-states for $N_2O^+$ along the N–N bond length and N–N–O angle, where two brown sand clocks note the avoided crossing positions.

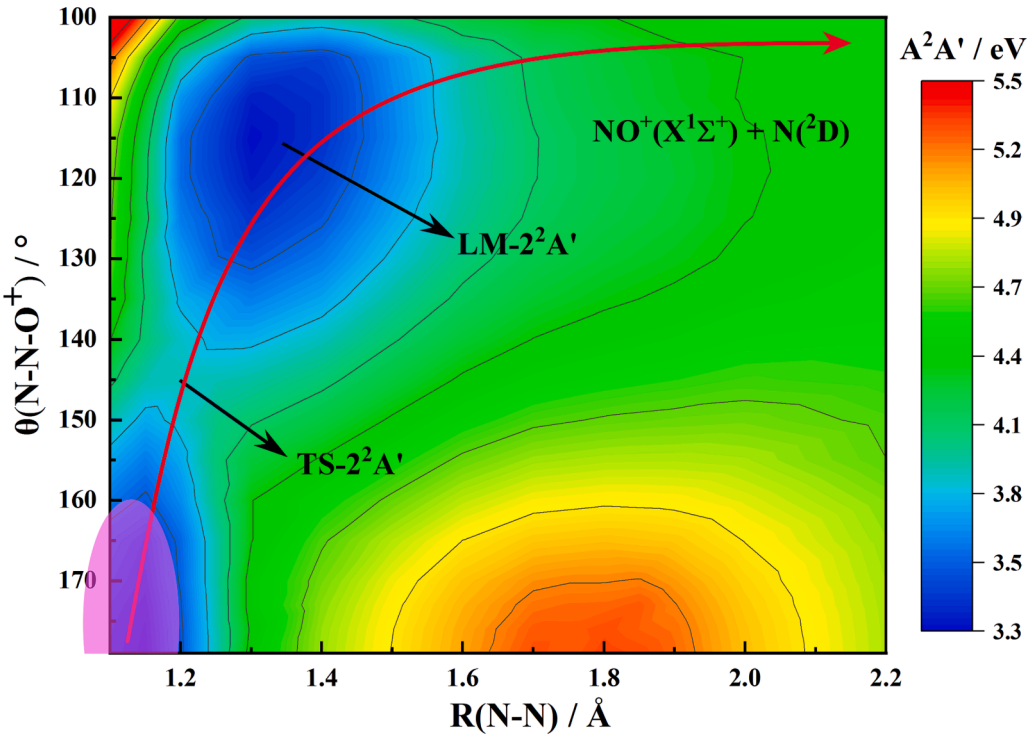


**Fig. 2.** CASPT2 potential energy surface of the $A^2A'$ state for $N_2O^+$ along the N–N bond and N–N–O angle, in which the Franck-Condon region is marked in purple. (For interpretation of the references to colour in this figure legend, the reader is referred to the web version of this article.)

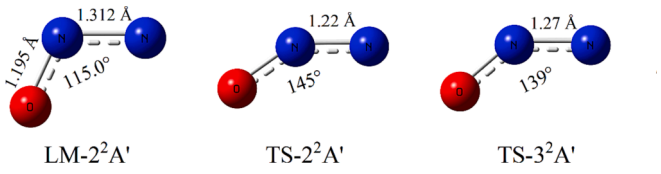


**Fig. 3.** Optimized geometries of local minima and transition states along the N–N bond fission of $N_2O^+$ in the $A^2A'$ and $B^2A'$ states at the CASPT2/cc-pVQZ level of theory.

this new path, the N–NO bond breaking will produce the rotationally excited $NO^+$ fragment. In summary, the calculated potential energy surface of $A^2\Sigma^+$ proposes a new and more favorable decomposition pathway of $N_2O^+$ in bent geometry, in addition to the linear one mentioned in previous calculation [40].

### 3.4. Potential energy surfaces of the $B^2A'(3^2A')$ and $B^2A''(2^2A'')$ sub-states

According to the significantly different geometries of the $B^2A'$ and $B^2A''$ sub-states, they might have different dissociation behaviors. Thus, we discuss them separately below. Fig. 4 shows the calculated $B^2A'$ and $B^2A''$ potential energy surfaces along N–N bond and N–N–O bond angle coordinates. Apparently, these two sub-states exhibit different patterns on the adiabatic dissociation potential energy surfaces.

As shown in Fig. 4a, there is a very high barrier (~1.50 eV at CASPT2 level) for $N_2O^+(B^2A')$ ions to dissociate along the linear N–NO bond fission, while the potential energy surface of $B^2A'$ exhibits much flat along the bending coordinate in the FC region although its global minimum is linear. As indicated with red arrow in Fig. 4a, the minimum energy path (MEP) of the N–NO bond breaking of $N_2O^+(B^2A')$ undergoes a low barrier,

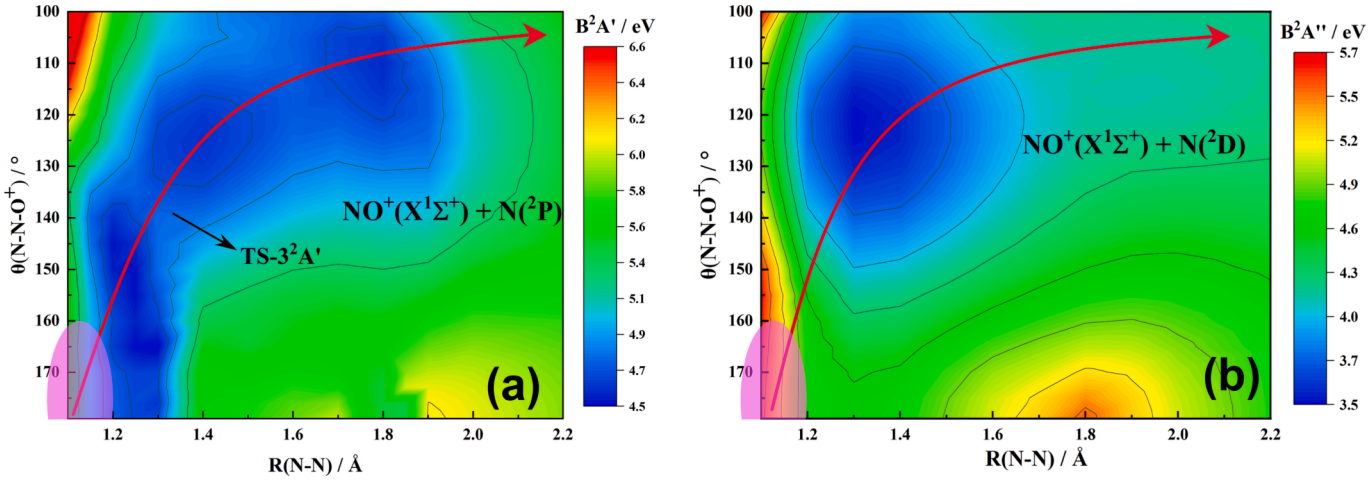


**Fig. 4.** CASPT2 potential energy surfaces of $B^2A'$ (a) and $B^2A''$ (b) sub-states for $N_2O^+$ along the N–N bond and N–N–O angle, in which the Franck-Condon region is marked in purple.

TS-3$^2$A', with the height of 0.27 eV. In TS-3$^2$A', the bond angle is 139° and the R(N–NO) length is 1.27 Å (Fig. 3). Along this MEP, the driving force of potential energy surface near FC region drives the molecule from linear to bent geometry, while the N–N bond length retains almost unchanged. Once the potential barrier is crossed, $N_2O^+$ can directly decompose to $NO^+(X^1\Sigma^+)$ and $N(^2P)$ fragments in bent geometry with the bond angle of ~ 115°. As a result, rotationally excited $NO^+$ fragment ions are produced, in line with experimental conclusions [15,34,37]. In addition, this new mechanism can explain the experimental phenomenon [37] that the proportion of the $NO^+(X^1\Sigma^+)$ + $N(^2P)$ channel increased with the excitation energy in decomposition of the $B^2\Pi$ state.

In comparison to $B^2A'$, the $B^2A''$ sub-state shows a character of steep repulsive potential in the FC region as shown in Fig. 4b. The repulsive potential drives the molecule to bend rapidly prior to dissociation once formed in the FC region. A global minimum is located at the middle of the MEP, in which the bond angle, the R(N–NO) and R(N–N–O) lengths are 121.4°, 1.315 and 1.197 Å, respectively, as shown in Table 2. The second dissociation limit of $NO^+(X^1\Sigma^+)$ + $N(^2D)$ adiabatically correlates with $B^2A''$ via a low barrier of ~ 0.4 eV height. According to that this barrier is much lower than the initial energy in FC ionization, the adiabatic N–NO bond breaking in bent geometry readily occurs for $N_2O^+$ in the $B^2A''$ state as indicated by red arrow in Fig. 4b. Notably, the discrete dissociation behaviors of $B^2A'$ and $B^2A''$ in $C_s$ symmetry are never noticed previously, despite providing more clues to understand the decomposition mechanism of $N_2O^+(B^2\Pi)$. In addition, as mentioned above, the $B^2A'$ sub-state is dominantly produced in photoionization to $N_2O^+(B^2\Pi)$, and hence the overall dissociation behavior of $B^2\Pi$ mainly occurs along the $B^2A'$ adiabatic potential energy surface rather than the $B^2A''$ one.

### 3.5. Compared with the potential energy surfaces of $N_3$ as the isoelectronic species

It is worthwhile to compare the multistate PESs of $N_2O^+$ and its isoelectronic $N_3$ due to foreseeable similarity. Varandas et al. [52–54] and Varga et al. [55] reported *ab initio* PESs at the CASSCF, CASPT2 and MRCI (Q) levels. Interestingly, the PESs of these two isoelectronic molecules show a high degree of consistency. The ground state ($^2\Pi_g$) of $N_3$ shows similar characteristics to $N_2O^+$, that holds a linear stationary structure and adiabatically correlates with the second dissociation limit, $N(^2D) + N_2$ [53]. The first excited state, $^2\Sigma_g^+$, of $N_3$ (corresponding to the $A^2\Sigma^+$ state of $N_2O^+$) also has a linear minimum but correlates with the $N(^2D)$ + $N_2$ dissociation limit in bent geometry [54], which is similar to our current conclusion that the $A^2A'(A^2\Sigma^+)$ state of $N_2O^+$ adiabatically links with the lower dissociation limit of $NO^+(X^1\Sigma^+)$ + $N(^2D)$ in bent geometry. The higher state, $^2\Pi_u$, of $N_3$ (corresponding to the $B^2\Pi$ state of $N_2O^+$) can dissociate to the $N(^2P)$ and $N_2$ fragments in linear configuration, however, the strong coupling with upper states causes the $2^2A''(^2\Pi_u)$ sub-state to dissociate along the lower $N(^2D)$ + $N_2$ channel in bent geometry [53]. Furthermore, the stationary structure of $2^2A''(^2\Pi_u)$ of $N_3$ is located at 120° [54], which is close to 121.4° of $2^2A''(^2\Pi_u)$ of $N_2O^+$. All these similarities provide indirect evidence for the reliability of current calculations. In addition, the multistate PESs of $N_3$ further confirm that the bending configuration is of paramount importance in calculating potential energy surfaces of the decomposition of triatomic molecules.

### 3.6. Dissociation mechanisms for $N_2O^+$ in the $A^2\Sigma^+$ and $B^2\Pi$ states

Based on the above potential energy surfaces, adiabatic decomposition mechanism of $N_2O^+$ in the $A^2\Sigma^+$ and $B^2\Pi$ states can be qualitatively uncovered. Moreover, the strong SOC value (53.8 $cm^{-1}$) between $A^2\Sigma^+(2^2A')$ and $1^4A''(1^4\Pi)$ was given by Huang et al. [40] Therefore, taking into account interactions among those doublet states with same symmetry (e.g. avoided crossing) and SOC to quartet states, ro-vibrational distributions of the $NO^+$ fragment observed in experiments can be reasonably illuminated.

For the $N_2O^+(A^2\Sigma^+)$ decomposition, $NO^+$ fragment ions were observed with three ro-vibrational distributions in experiments [27], i.e. $N(^4S)$ + $NO^+$(vibrationally excited), $N(^2D)$ + $NO^+$(rotationally "cold") and $N(^2D)$ + $NO^+$(rotationally "hot"). The appearance of the $NO^+(X^1\Sigma^+)$ + $N(^4S)$ channel is assuredly attributed to the coupling of spin states from the linear $A^2\Sigma^+$ to the bent $1^4A''(1^4\Pi)$ quartet state, leading to vibrational "hot" $NO^+(X^1\Sigma^+)$ fragments. Besides, as proposed by Huang et al. [40], $A^2\Sigma^+(2^2A')$ can undergo bent deformation to $1^4A''$ and then reach the $1^2A''(X^2\Pi)$ state via strong SOCs (53.8 $cm^{-1}$ for $A^2\Sigma^+(2^2A') \rightarrow 1^4A''(1^4\Pi)$, and 70.9 $cm^{-1}$ for $1^4A'' \rightarrow 1^2A''(X^2\Pi)$) at their own minimum energy crossing points, and further adiabatically dissociate along $1^2A''(X^2\Pi)$ to product $NO^+(X^1\Sigma^+)$ and $N(^2D)$ fragments. According to the linear structure of $1^2A''$, rotationally "cold" $NO^+$ fragments are produced. Moreover, following the current conclusions, the MEP on the $A^2\Sigma^+(2^2A')$ potential energy surface (Fig. 2) shows an irrefutable mechanism of adiabatic decomposition, providing a perfect explanation for the production of rotationally excited $NO^+$ observed in experiments [27]. We would like to emphasize that it is a novel mechanism. In addition, owing to the existence of the local minimum (LM-2$^2$A'), we can imagine that the N–NO stretching and the bending vibrations can efficiently promote the branching ratio of this pathway, which is greatly consistent with the vibrational-dependence experimental results [27]. Therefore, the overall decomposition of $N_2O^+(A^2\Sigma^+)$ can be summarized as the following:

The decomposition of $N_2O^+(B^2\Pi)$ is much complicated. Both $NO^+(X^1\Sigma^+)$ + $N(^2D)$ and $NO^+(X^1\Sigma^+)$ + $N(^2P)$ dissociation channels were both observed in experiments, and the former was dominant [56]. Moreover, ro-vibrational population of the $NO^+$ fragment strongly implied that significant bending took place prior to N–NO bond breaking [37]. As described in Section 3.4, the $NO^+(X^1\Sigma^+)$ + $N(^2P)$ channel adiabatically correlates with the $B^2A'$ sub-state in bent geometry via a low barrier, while the $B^2A''$ is dissociative with the products of $NO^+(X^1\Sigma^+)$ and $N(^2D)$. According to that the $B^2A'$ sub-state is predominantly produced in FC photoionization, the $NO^+(X^1\Sigma^+)$ + $N(^2P)$ dissociation channel observed in experiments is attributed to the $B^2A'$ adiabatic decomposition. Besides, both Chambaud et al.'s [38] and our calculations propose a non-adiabatic dissociation pathway of $N_2O^+(B^2\Pi)$, that the $B^2A'(B^2\Pi)$ state can couple to $A^2A'(A^2\Sigma^+)$ with bending vibration at near equilibrium geometry of $B^2A'$, then adiabatically dissociate to $NO^+(X^1\Sigma^+)$ and $N(^2D)$ along the $A^2A'$ potential energy surface. Considering that the $A^2A'(A^2\Sigma^+)$ decomposition can produce rotationally "hot" and "cold" $NO^+$ fragment ion and $N(^2D)$ atom, the coupling from $A^2A'(A^2\Sigma^+)$ will induce $N_2O^+(B^2\Pi)$ to dissociate into $NO^+(X^1\Sigma^+)$ with bimodal rotational distributions and $N(^2D)$ atom. In summary, we attribute the $NO^+(X^1\Sigma^+)$ + $N(^2D)$ production path observed in experiments [37] to the non-adiabatic decomposition of

$$N_2O^+\left(A^2\Sigma^+, linear\right)\begin{cases} \overset{spin-orbit}{\rightarrow} N_2O^+\left(1^4A'', bent\right)\rightarrow N\left(^4S\right)+NO^+\left(X^1\Sigma^+, vibrationalexcited\right) \\ \overset{spin-orbit}{\rightarrow} N_2O^+\left(1^4A'', bent\right)\overset{spin-orbit}{\rightarrow}\left(N_2O^+\left(1^2A''\right)\left(X^2\Pi\right), linear\right)\rightarrow N\left(^2D\right)+NO^+\left(X^1\Sigma^+, rotationally\ ^{"}cold^{"}\right) \\ \overset{Isomerization}{\rightarrow} N_2O^+\left(A^2\Sigma^+, bent\right)\rightarrow N\left(^2D\right)+NO^+\left(X^1\Sigma^+, rotationally\ ^{"}hot^{"}\right) \end{cases}$$

$B^2A'$ via coupling to $A^2A'(A^2\Sigma^+)$ and breaking the N–NO bond. The following scheme briefly summarizes the above mechanisms:

$$N_2O^+\left(B^2A^{'}\left(B^2\Pi\right), linear\right)\begin{cases}\overset{Isomerization}{\rightarrow} N_2O^+\left(B^2A^{'}\left(B^2\Pi\right), bent\right)\rightarrow N\left(^2P\right)+NO^+\left(X^1\Sigma^+, rotationally\ ^{"}hot^{"}\right)\\ \overset{avoidedcrossing}{\rightarrow} N_2O^+\left(A^2A^{'}\left(A^2\Sigma^+\right), linear\right)\rightarrow\cdots\rightarrow N\left(^2D\right)+NO^+\left(X^1\Sigma^+\right)\end{cases}$$

Last but not least, although the current calculation levels are not sufficiently accurate to quantitatively describe full features on the $A^2\Sigma^+$ and $B^2\Pi$ potential energy surfaces, and in the absence of quantum chemical dynamic calculations, the MEP is only able to offer a possibility of the adiabatic dissociation mechanism, we would like to emphasize that the current study provides some important clues of the bent potential energy surfaces, which can point to the direction for quantitative calculations in future.

## 4. Conclusion

Through calculating potential energy surfaces of $N_2O^+$ cations along the N–N bond length and the N–N–$O^+$ angle coordinates, we re-investigate decomposition mechanisms of $N_2O^+$ cations in the $A^2\Sigma^+$ and $B^2\Pi$ states. In comparison to previous mechanisms in linear geometry [38], more complicated couplings are confirmed, which causes new dissociation pathways for the N–NO bond fission of $N_2O^+$. In these two states, adiabatic and non-adiabatic decomposition pathways compete with each other, resulting in the changes of the abundance and ro-vibrational distribution of products. The adiabatic correlation between these two states and the dissociation limits of $NO^+(X^1\Sigma^+)$ + $N(^4S)$, $NO^+(X^1\Sigma^+)$ + $N(^2D)$, and $NO^+(X^1\Sigma^+)$ + $N(^2P)$ are clarified.

Notably, a novel adiabatic decomposition path of $A^2A'(A^2\Sigma^+)$ state is found in bent geometry. According to its lower barrier, this thermodynamically allowed N–N bond fission is assigned to form the rotationally excited $NO^+(X^1\Sigma^+)$ and $N(^2D)$ fragments. Moreover, the respective contributions of the A' and A" components split from the linear $B^2\Pi$ state are clarified separately. Considering avoided crossing among doublet states with same symmetry and SOC to quartet states, ro-vibrational distribution of $NO^+$ fragment observed in experiments is reasonably elucidated. The current conclusions exhibit a nice example for an in-depth study of dissociation dynamics of polyatomic molecules.

## CRediT authorship contribution statement

**Yan Chen:** Formal analysis, Methodology, Investigation, Writing – original draft. **Xiangkun Wu:** Formal analysis, Methodology, Investigation. **Tongpo Yu:** Resources, Validation. **Xiaoguo Zhou:** Supervision, Funding acquisition, Conceptualization, Writing – review & editing. **Bing Yan:** Supervision, Funding acquisition, Software. **Shilin Liu:** Supervision, Funding acquisition.

## Declaration of Competing Interest

The authors declare the following financial interests/personal relationships which may be considered as potential competing interests: Xiaoguo Zhou reports financial support was provided by National Natural Science Foundation of China. Xiaoguo Zhou reports financial support was provided by Fundamental Research Funds for the Central Universities.

## Data availability

Data will be made available on request.

## Acknowledgements

The financial supports of the National Natural Science Foundation of China (Nos. 21903079, 12274178, and 22073088) are gratefully acknowledged. X. Zhou is also grateful for the support of the Fundamental Research Funds for the Central Universities.

## References

[1] W. Tsang, J.T. Herron, Chemical kinetic data-base for propellant combustion. 1. Reactions involving NO, NO2, HNO, HNO2, HCN and N2O, J. Phys. Chem. Ref. Data 20 (4) (1991) 609–663.
[2] H.Q. Tian, R.T. Xu, J.G. Canadell, et al., A comprehensive quantification of global nitrous oxide sources and sinks, Nature 586 (7828) (2020) 248–256.
[3] V. Lew, E. McKay, M. Maze, Past, present, and future of nitrous oxide, Brit. Med. Bull. 125 (1) (2018) 103–119.
[4] C.-Y. Ng, T. Baer, I. Powis, Unimolecular and bimolecular ion-molecule reaction dynamics, Wiley, 1994.
[5] C.R. Brundle, D.W. Turner, Studies on the photoionisation of the linear triatomic molecules: N2O, COS, CS2 and CO2 using high-resolution photoelectron spectroscopy, Int. J. Mass Spectrom. 2 (3) (1969) 195–220.
[6] D.W. Turner, D.P. May, Franck—Condon Factors in Ionization: Experimental Measurement Using Molecular Photoelectron Spectroscopy. II, J. Chem. Phys. 46 (3) (1967) 1156–1160.
[7] J.M. Hollas, T.A. Sutherley, The geometries of the X˜ and Ã states of N2O+ from photoelectron spectroscopy compared with those derived from the emission spectrum, Chem. Phys. Lett. 21 (1) (1973) 167–169.
[8] M.J. Weiss, High resolution He I photoelectron spectroscopy of the C2Σ+ state of N2O, Chem. Phys. Lett. 39 (2) (1976) 250–251.
[9] P.M. Dehmer, J.L. Dehmer, W.A. Chupka, Effects of vibronic interaction and autoionization on the photoelectron spectrum of N2O, J. Chem. Phys. 73 (1) (1980) 126–133.
[10] R. Locht, G. Caprace, J. Momigny, The dissociative ionization of nitrous oxide. A comparison between electroionization and HeI and NeI photoionization, Chem. Phys. Lett. 111 (6) (1984) 560–565.
[11] I. Nenner, P.M. Guyon, T. Baer, et al., A threshold photoelectron–photoion coincidence study of the N2O+ dissociation between 15 and 20.5 eV, J. Chem. Phys. 72 (12) (1980) 6587–6592.
[12] M. Richard-Viard, O. Atabek, O. Dutuit, et al., Experimental evidence of vibrational mode selectivity in the indirect predissociation of N2O+ A2Σ+. Energy distribution of the diatomic fragment and comparison with a model prediction, J. Chem. Phys. 93 (12) (1990) 8881–8892.
[13] M. Richard-Viard, A. Delboulbé, M. Vervloet, Experimental study of the dissociation of selected internal energy ions produced in low quantities: application to N2O+ ions in the Franck-Condon gap and to small ionic water clusters, Chem. Phys. 209 (2) (1996) 159–167.
[14] S.-Y. Chiang, C.-I. Ma, Fragmentation of Vibrationally Selected N2O+ in State C2Σ + from Measurements of Threshold Photoelectron Photoion Coincidence, Chem. A Eur. J. 104 (10) (2000) 1991–1996.
[15] X.F. Tang, X.G. Zhou, B.L. Qiu, et al., New insight into dissociative photoionization of N2O at similar to 20 eV using threshold photoelectron-photoion coincidence velocity imaging, J. Electron Spectrosc. Relat. Phenom. 196 (2014) 43–48.
[16] R.T. Wiedmann, E.R. Grant, R.G. Tonkyn, et al., High-resolution threshold photoionization of N2O, J. Chem. Phys. 95 (2) (1991) 746–753.
[17] W. Kong, D. Rodgers, J.W. Hepburn, Pulsed field ionization threshold photelectron spectroscopy of the fluorescing N2O+ (A2Σ+) state, Chem. Phys. Lett. 221 (3) (1994) 301–306.
[18] W. Chen, J. Liu, C.Y. Ng, Vacuum Ultraviolet Pulsed Field Ionization−Photoelectron Study for N2O+ in the Energy Range of 16.3−21.0 eV, Chem. A Eur. J. 107 (40) (2003) 8086–8091.
[19] H. Xu, Y. Guo, Q. Li, et al., Spectroscopic study of N2O+(A 2Σ+) by photofragment excitation spectrum, J. Chem. Phys. 119 (22) (2003) 11609–11614.
[20] J.L. Olivier, R. Locht, J. Momigny, A dissociative electroionization study of nitrous oxide. The NO+ and N2+ dissociation channels, Chem. Phys. 68 (1) (1982) 201–211.
[21] J.L. Olivier, R. Locht, J. Momigny, The dissociative electroionization of nitrous oxide. The O+ dissociation channel, Int. J. Mass Spectrom. 46 (1983) 251–254.
[22] J.L. Olivier, R. Locht, J. Momigny, A dissociative electroionization study of nitrous oxide. The O+ and N+ dissociation channels, Chem. Phys. 84 (2) (1984) 295–309.

[23] P. Coppens, J. Smets, M.G. Fishel, et al., Mass spectrometric study of the photoionization of nitrous oxide in the wavelength interval 1000–600 Å, Int. J. Mass Spectrom. 14 (1) (1974) 57–74.
[24] J. Berkowitz, J.H.D. Eland, Photoionization of N2O: Mechanisms of photoionization and ion dissociation, J. Chem. Phys. 67 (6) (1977) 2740–2752.
[25] R. Locht, G. Hagenow, K. Hottmann, et al., Photoionization mass spectrometry of kinetic energy-selected ions. An ion retarding potential difference method applied to NO+ and O+ from N2O, Chem. Phys. 151 (1) (1991) 137–148.
[26] H. Xu, Y. Guo, Q. Li, et al., Channel switching effect in photodissociating N2O+ ion at 312.5 nm, J. Chem. Phys. 121 (7) (2004) 3069–3073.
[27] H. Wang, X. Zhou, S. Liu, et al., Predissociation dynamics of N2O+ at the A (2) Sigma(+) state: Three pathways to form NO+((1)Sigma(+)) revealed from ion velocity imaging, J. Chem. Phys. 132 (24) (2010), 244309.
[28] S. Abed, M. Broyer, M. Carré, et al., High-resolution spectroscopy of N2O+ in the near ultraviolet using fiblas (fast-ion-beam laser spectroscopy), Chem. Phys. 74 (1) (1983) 97–112.
[29] M. Larzillière, C. Jungen, Fast ion beam laser spectroscopy of N2O+, Mol. Phys. 67 (4) (1989) 807–837.
[30] J.H.D. Eland, Predissociation of N2O+ and COS+ ions studied by photoelectron-photoion coincidence spectroscopy, Int. J. Mass Spectrom. 12 (4) (1973) 389–395.
[31] B. Brehm, R. Frey, A. Küstler, et al., Kinetic energy release in ion fragmentation: N2O+, COS+ and CF4+ decays, Int. J. Mass Spectrom. 13 (3) (1974) 251–260.
[32] E. Kinmond, J.H.D. Eland, L. Karlsson, Dissociation of N2O+ ions from the valence states reached by one-photon photoionisation11Dedicated to Professor Michael T. Bowers on the occasion of his 60th birthday, Int. J. Mass Spectrom. 185–187 (1999) 437–447.
[33] X. Tang, M. Niu, X. Zhou, et al., NO+ formation pathways in dissociation of N2O+ ions at the C-2 Sigma(+) state revealed from threshold photoelectron-photoion coincidence velocity imaging, J. Chem. Phys. 134 (5) (2011), 054312.
[34] M. Lebech, J.C. Houver, D. Dowek, et al., Dissociative photoionization of N2O in the region of the N2O+(B 2Π) state studied by ion–electron velocity vector correlation, J. Chem. Phys. 120 (17) (2004) 8226–8240.
[35] M. Lebech, J.C. Houver, D. Dowek, et al., Dissociative photoionization of N2O in the region of the N2O+(C 2Σ+) state, studied by ion–electron velocity vector correlation, J. Chem. Phys. 117 (20) (2002) 9248–9257.
[36] M.A. Gharaibeh, D.J. Clouthier, A laser-induced fluorescence study of the jet-cooled nitrous oxide cation (N2O+), J. Chem. Phys. 136 (4) (2012), 044318.
[37] Z.F. Zhou, H. Liang, Z.F. Hua, et al., N-loss photodissociation dynamics of N2O+(B-2 Pi) near the NO+((1)Sigma(+)) + N(2P) dissociation limit, J. Chem. Phys. 150 (22) (2019), 226101.
[38] G. Chambaud, H. Gritli, P. Rosmus, et al., The ion-molecule reaction O+ (4S) + N2 (X1Σ+) → NO+ (X1Σ+, v′) + N(4S) and the predissociation of the A2Σ+ and B2Π states of N2O+, Mol. Phys. 98 (21) (2000) 1793–1802.
[39] H.-B. Chang, Q. Meng, M.-B. Huang, et al., A theoretical study on the mechanisms of the N-2(X-1 Sigma(+)(g)) + O+(S-4(u)) reaction involving the 1(4) A '' and X-2 Pi states of the N2O+ ion and the predissociation of the X-2 Pi state, Mol. Phys. 108 (16) (2010) 2137–2145.
[40] Q.Y. Meng, H.B. Chang, M.B. Huang, et al., Theoretical studies on N-loss predissociation mechanisms of N2O+ (A I-2 (+)) pound in C (s) symmetry, Theor. Chem. Acc. 128 (3) (2011) 359–365.
[41] O. Yazidi, A. Ben Houria, J.S. Francisco, et al., Electronic states, conical intersections, and spin-rovibronic spectroscopy of the nitrogen oxide sulfide radical, J. Chem. Phys. 138 (10) (2013), 104318.
[42] T. Trabelsi, S. Ben Yaghlane, M.M. Al Mogren, et al., HNS+ and HSN+ cations: Electronic states, spin-rovibronic spectroscopy with planetary and biological implications, J. Chem. Phys. 145 (8) (2016), 084307.
[43] Z.W. Luan, Y.L. Fu, Y.X. Tan, et al., Observation of Competitive Nonadiabatic Photodissociation Dynamics of H2S+ Cations, J. Phys. Chem. Lett. 13 (34) (2022) 8157–8162.
[44] H.-J. Werner, P.J. Knowles, G. Knizia, et al., MOLPRO, version 2021.3, a package of *ab initio* programs, 2021.
[45] J. Finley, P.-Å. Malmqvist, B.O. Roos, et al., The multi-state CASPT2 method, Chem. Phys. Lett. 288 (2) (1998) 299–306.
[46] T.H. Dunning, Gaussian basis sets for use in correlated molecular calculations. I. The atoms boron through neon and hydrogen, J. Chem. Phys. 90 (2) (1989) 1007–1023.
[47] H. Koppel, L.S. Cederbaum, W. Domcke, Strong non-condon effects induced by electron correlation: N2O+, Chem. Phys. 69 (1–2) (1982) 175–183.
[48] J.H. Callomon, F. Creutzberg, The electronic emission spectrum of ionized nitrous oxide, N2O+ : Ã2Σ+—X2Π, Philos. Trans. Royal Soc. A 277 (1266) (1974) 157–189.
[49] K. Kimura, Handbook of HeI photoelectron spectra of fundamental organic molecules, Halsted Press, 1981.
[50] H. Herburger, U. Hollenstein, J.A. Agner, et al., PFI-ZEKE-photoelectron spectroscopy of N2O using narrow-band VUV laser radiation generated by four-wave mixing in Ar using a KBBF crystal, J. Chem. Phys. 151 (14) (2019), 144302.
[51] R.G. Orth, R.C. Dunbar, Photodissociation of nitrous oxide cation, J. Chem. Phys. 66 (4) (1977) 1616–1620.
[52] B.R.L. Galvao, A.J.C. Varandas, Accurate Double Many-Body Expansion Potential Energy Surface for N-3((4)A") from Correlation Scaled ab Initio Energies with Extrapolation to the Complete Basis Set Limit, J. Phys. Chem. A 113 (52) (2009) 14424–14430.
[53] B.R.L. Galvao, A.J.C. Varandas, Ab Initio Based Double-Sheeted DMBE Potential Energy Surface for N-3((2)A '') and Exploratory Dynamics Calculations, J. Phys. Chem. A 115 (44) (2011) 12390–12398.
[54] B.R.L. Galvao, P. Caridade, A.J.C. Varandas, N(S-4/D-2)+N-2: Accurate ab initio-based DMBE potential energy surfaces and surface-hopping dynamics, J. Chem. Phys. 137 (22) (2012).
[55] Z. Varga, D.G. Truhlar, Potential energy surface for high-energy N + N-2 collisions, PCCP 23 (46) (2021) 26273–26284.
[56] M. Lebech, J.C. Houver, D. Dowek, et al., Molecular frame photoelectron emission in the presence of autoionizing resonances, Phys. Rev. Lett. 96 (7) (2006), 073001.